Featured in Physics

Optical Absorption Spectroscopy Probes Water Wire and Its Ordering in a Hydrogen-Bond Network

Fujie Tang,[1,2] Diana Y. Qiu,[3,*] and Xifan Wu[1,†]

[1]*Department of Physics, Temple University, Philadelphia, Pennsylvania 19122, USA*
[2]*Pen-Tung Sah Institute of Micro-Nano Science and Technology, Tan Kah Kee Innovation Laboratory (IKKEM), Xiamen University, Xiamen, 361005, China*
[3]*Department of Materials Science, Yale University, New Haven, Connecticut 06520, USA*

(Received 21 August 2024; revised 23 November 2024; accepted 17 December 2024; published 5 March 2025)

Water wires, quasi-one-dimensional chains composed of hydrogen-bonded (H-bonded) water molecules, play a fundamental role in numerous chemical, physical, and physiological processes. Yet direct experimental detection of water wires has been elusive so far. Based on advanced *ab initio* many-body theory that includes electron-hole interactions, we report that optical absorption spectroscopy can serve as a sensitive probe of water wires and their ordering. In both liquid and solid water, the main peak of the spectrum is discovered to be a charge-transfer exciton. In water, the charge-transfer exciton is strongly coupled to the H-bonding environment where the exciton is excited between H-bonded water molecules with a large spectral intensity. In regular ice, the spectral weight of the charge-transfer exciton is enhanced by a collective excitation occurring on proton-ordered water wires, whose spectral intensity scales with the ordering length of water wire. The spectral intensity and excitonic interaction strength reaches its maximum in ice XI, where the long-range ordering length yields the most pronounced spectral signal. Our findings suggest that water wires, which widely exist in important physiological and biological systems and other phases of ice, can be directly probed by this approach.

DOI: 10.1103/PhysRevX.15.011048

Subject Areas: Chemical Physics, Computational Physics, Condensed Matter Physics

I. INTRODUCTION

In liquid water and crystalline ice, water molecules construct an extended hydrogen-bond (H-bond) network in the condensed phase. Besides its tetrahedral structural motif, these H bonds can form persistent, extended networks that act as a sort of highway for charge, energy, and information. These networks, known as "water wires," play an essential role across numerous physical, chemical, and physiological processes [1–8]. In liquid environments, water wires under biological confinement are believed to conduct both information and nutrition in a living cell [3,5,6,8,9]. While bulk water lacks a persistent water wire, it has been repeatedly proposed that a transient water wire facilitates proton transfer in water—a process that underlies acid-base chemistry [4,10–16]. In crystalline ice, the emergence of proton ordering on water wires was found to prelude the phase transition from ordinary ice to ferroelectric ice [1,7].

Although playing a crucial role in facilitating dynamical processes and phase transitions, the evidence for the existence of water wires remains largely circumstantial. These structures are presumed necessary to facilitate transport processes observed experimentally in aqueous environments, yet their precise molecular structure has not been directly observed to date. This is because characterization demands that the experiment detects not only the existence of H bonds, but also the intricate and dynamical network of correlations between H bonds while chains are being formed. In conventional scattering experiments, only positional information can be extracted [17,18]. Optical spectroscopy is, in principle, sensitive to both positional and angular distributions [19–21], but, so far, previous works have mainly relied on x-ray absorption spectroscopy to probe the structure of the H-bond network [22–27]. This core-level spectroscopy generates an intramolecular exciton that is too strongly localized on the individual excited water molecules to convey detailed information about the H-bond network [24–26]. Its spectrum carries little

*Contact author: diana.qiu@yale.edu
†Contact author: xifanwu@temple.edu

information on how the H bonds are interconnected, and it is, thus, insensitive to the existence of water wires. Extending the characterization to optical spectroscopy, which excites the more delocalized valence electrons, has potential to offer greater access to the H-bond network.

Despite the potential of optical absorption as a probe of delocalized states across H bonds, the correlation of spectral features with the underlying H-bond network is immensely complex, requiring quantitatively accurate descriptions of delocalized correlated electron-hole excitations in a theoretical environment that accurately captures both the H bonds and the many-electron interactions present in the condensed phase. In this article, we develop such a theoretical platform and report that optical absorption spectroscopy, a widely used experimental technique, can serve as a sensitive probe of the water wire. We justify our approach by a novel assignment of the experimentally observed spectral features to the structural signature of the H-bond network. Our theoretical analyses are based on *ab initio* calculations within a many-body framework that takes into account dynamical many-electron screening effects, the single-particle self-energy, and electron-hole interactions. The absorption of UV light creates charge-transfer excitons across H bonds that give rise to a distinct spectral feature around approximately 8 eV [28–35]. In bulk liquid water, the dynamical breaking and reformation of H bonds on a timescale of picoseconds [36–38] broadens the spectral feature, while in regular ice the spectral feature is much more pronounced than that in water due to the emergence of water wires with intact H bonds. On a proton-ordered water wire, the aligned electric dipoles along the ordering direction facilitate a collective excitation of charge-transfer excitons leading to a dramatic enhancement of the optical transition strength. As the ordering length of the water wire increases, the excitonic effects due to the collective excitation of charge-transfer excitons is enhanced as well, reaching a maximum oscillator strength and exciton binding energy in ice XI, where the water wires exhibit long-range order [1,7].

II. METHODS

Our theoretical calculations use the *ab initio GW* plus Bethe Salpeter equation (*GW*-BSE) method within many-body perturbation theory as implemented in the BerkeleyGW software package [39–41]. The molecular structure is modeled by using machine-learning deep potential molecular dynamics simulations, where the model is trained at the level of the hybrid meta-GGA (SCAN0) exchange-correlation (XC) functional [42]. The quasiparticle wave functions are computed by hybrid density functional theory (DFT) at the level of the Perdew, Burke, and Ernzerhof (PBE0) XC functional [43–45]. The use of hybrid DFT functional, for both molecular and electronic structures, mitigates the errors due to self-interaction and missing derivative discontinuity [46–48], i.e., common drawbacks in conventional DFT approaches which lead to an artificially stronger H-bonding strength and overestimated electron-hole attractions in water and ice.

The configurations of liquid water are extracted from a path-integral deep potential molecular dynamics (PI-DPMD) simulation trajectory. The deep potential model was trained on the DFT data obtained with the hybrid strongly constrained and appropriately normed (SCAN0) functional [42]. The cubic cells contain 32 water molecules, while the size of the supercell is adjusted to have the same density in experiment. PI-DPMD simulation is performed in the NVT ensemble at $T = 300$ K using periodic boundary conditions with the cell sizes fixed at 9.708 Å. The Feynman paths are represented by eight-bead ring polymers coupled to a color noise generalized Langevin equation thermostat (i.e., PIGLET) [49,50]. The total length of PI-DPMD simulation used well equilibrated approximately 500-ps-long trajectories. After we obtain the MD trajectory, we use a score function (see Sec. I in Supplemental Material [51]) to pick out two representative snapshots for the following *GW*-BSE calculation. For the configurations used in the ice I*h* calculation, we first generate eight initial geometries of ice I*h* following the *ice rules* [52,53] with different random seeds, in which the protons are in a disorder structure. The supercell contains 64 water molecules with a size of $a = 8.9873$ Å, $b = 15.5665$ Å, and $c = 14.6763$ Å. For the ice XI, the number of water molecules and cell size are set to the same as the setting used in the ice I*h*. We optimize the structure of ice XI at 0 K at the SCAN0 level of theory before used for the *GW*-BSE calculation.

The *GW*-BSE calculations are done with the BerkeleyGW package [41]. We first construct the wave functions as the starting point for our *GW*-BSE calculation using DFT at the level of the hybrid generalized gradient approximations (GGA) of PBE0 [43–45] with 25% of Hartree-Fock exchange energy, as implemented in the Quantum ESPRESSO package [54]. We choose PBE0 to reduce the overestimated charge-transfer effects of induced by the ground state theory [55,56]. The multiple-projector norm-conserving pseudopotentials that match the potentials for oxygen and hydrogen are generated by using the ONCVPSP package [57]. The plane-wave kinetic energy cutoff is set to 85 Ry. The BSE calculation is done with 128 valence band states and 192 conduction band states for liquid water and 192 valence band states and 240 conduction band states for ice, which are enough to cover the energy range in which we are interested. For all the BSE calculations, we solve the electron-hole excitations within the *GW*-BSE approach in the Tamm-Dancoff approximation [40]. Further details of the calculations can be found in Sec. II in Supplemental Material [51]. We also calculate the real part of the dielectric function as well as the absorption coefficient spectra of liquid water and ice, reported in Sec. VII in Supplemental Material [51].

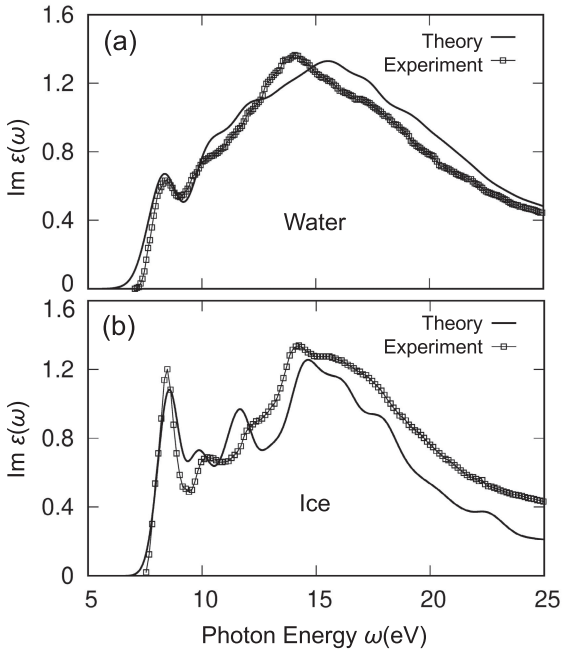

FIG. 1. The experimental and theoretical optical absorption spectra of (a) liquid water and (b) ice. The theoretical optical spectra of liquid water is generated by using the atomic configuration (32 H_2O) from a PI-DPMD simulation at 300 K, while the ice spectra are generated by using the atomic configuration (64 H_2O) from a DPMD simulation for ice Ih at 80 K. The theoretical spectra are aligned with experimental data with the position of first peak with a blueshift of approximately 0.6 eV (liquid water) and approximately 0.8 eV (ice), respectively. The experimental data are taken from Refs. [58,59] for water and ice, respectively.

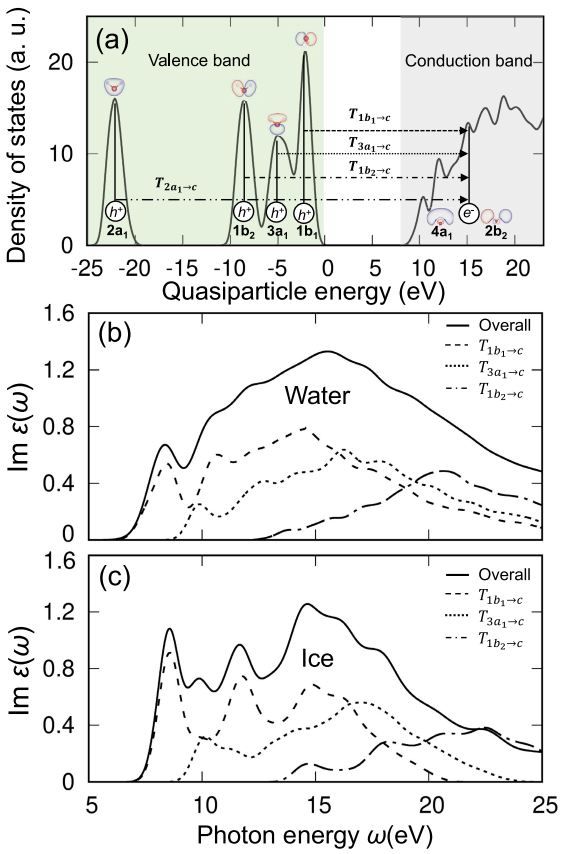

FIG. 2. (a) Schematic of band-to-band transitions contributing to the optical spectra: $\mathcal{T}_{1b_1\to c}$, between valence band states with $1b_1$ characteristic and conduction band states c; $\mathcal{T}_{3a_1\to c}$, between valence band states with $3a_1$ characteristic and conduction band states c; $\mathcal{T}_{1b_2\to c}$, between valence band states with $1b_2$ characteristic and conduction band states c; $\mathcal{T}_{2a_1\to c}$, between valence band states with $2a_1$ characteristic and conduction band states c. The black vertical lines mark the peak of the quasiparticle density of states. The theoretical optical spectra of liquid water (b) and ice (c) from the GW-BSE approach with all valence band states contribution (solid line) and with $\mathcal{T}_{1b_1\to c}$ transition only (dashed line), $\mathcal{T}_{3a_1\to c}$ transition only (dotted line), and $\mathcal{T}_{1b_2\to c}$ transition only (dash-dotted line). Note that the contribution from the transition $\mathcal{T}_{2a_1\to c}$ is zero.

III. RESULTS AND DISCUSSION

A. Theoretical optical spectra of liquid water and ice

We present our calculated optical absorption spectra for liquid water at 300 K and ice at 80 K in Figs. 1(a) and 1(b), respectively. The calculations are performed using the *ab initio* GW-BSE method [39–41]. Details of the calculation may be found in Secs. I and II in Supplemental Material [51]. For comparison, the recent experimental measurements from Refs. [58,59] are also shown in the same figure. The theoretical water and ice spectra are blueshifted by approximately 0.6 eV and approximately 0.8 eV, respectively, and both broadened by 0.4 eV with a Gaussian function to match the energy and width of the first peak in experiment. Clearly, an accurate agreement can be seen between experiments and theoretical predictions. In both water and ice, the absorption onset is dominated by a major absorption peak centered at approximately 8 eV followed by a more broadly distributed spectral feature at approximately 15 eV. Despite the similarities, ice is distinct from water in its spectrum. Compared to that in water, the spectrum of ice shows a much stronger absorption peak at approximately 8 eV together with more pronounced spectral features for the incident photon energy between approximately 8 eV and approximately 15 eV.

In the condensed phase, intermolecular interactions broaden molecular orbital energy levels into bands of finite width. Optical absorption spectroscopy probes dipole-allowed transitions between these bands as shown in Fig. 2(a). To understand the nature of the spectral features, we break down the absorption spectrum by contributions from specific band-to-band transitions. In water, the highest occupied bands are valence band states with $1b_1$, $3a_1$, $1b_2$, and $2a_1$ character, respectively, and the lowest unoccupied bands have characters $4a_1$ and $2b_2$, respectively. The

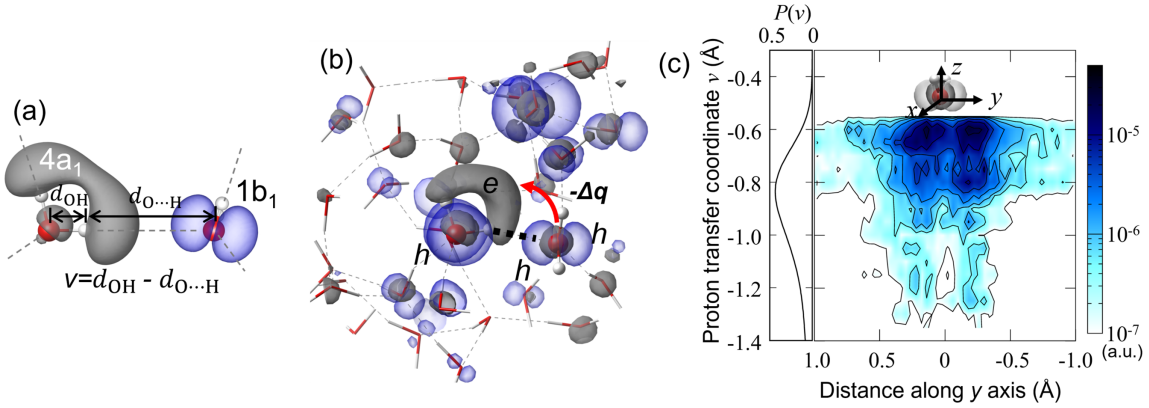

FIG. 3. (a) The schematic of the H bond and proton transfer coordinate ($\nu = d_{\mathrm{OH}} - d_{\mathrm{O\cdots H}}$). (b) Exciton corresponding to the first peak of the optical spectrum of the liquid water in real space. The real-space plot is the averaged electron and hole density of the exciton. The blue color denotes the hole density, while the gray color denotes the electron density. (c) The two-dimensional contour plot of the overlap between hole density and electron density ($\rho_h \times \rho_e$) with respect to the distance along the y axis (perpendicular to the plane of the water molecule) and the proton transfer coordinate. The proton transfer coordinate distribution is shown for reference. The x-z plane is parallel to the water molecule. The zero point of the y axis is set at the position of the oxygen atom.

schematic of the orbital character of water molecules is shown in Fig. 2(a). In the full calculation, all electron-hole pairs contribute to the spectra. We decompose the spectra into contributions from specific transitions by solving the BSE on a subspace with only selected orbitals, and we find that the full spectrum is well approximated by the solution on a subspace containing only the p orbital electrons near the Fermi level (i.e., the $1b_1$, $3a_1$, and $1b_2$ bands); see the details in Sec. IV in Supplemental Material [51].

In Fig. 2(a), we label the transitions between the valence and conduction bands that contribute to the optical absorption. Then, in Fig. 2(b), we show how each transition contributes to the overall optical absorption by restricting the calculation of the optical absorption spectrum to specific valence and conduction bands. From this, we see that in both liquid water and ice the first absorption peak around approximately 8 eV comes from transitions from valence states of $1b_1$ (or oxygen p) character. The broad feature at approximately 15 eV comes from the broadening of several distinct exciton peaks arising from transitions from $1b_1$ and $3a_1$ orbitals because of the dispersion of the oxygen p band in Fig. 2(a). The low-lying oxygen $2s$ valence band of $2a_1$ character does not contribute to the optical absorption spectrum in the current energy range.

B. Charge-transfer exciton strongly couples to H bond

The first absorption peak at approximately 8 eV, as shown in Fig. 3(a), exhibits charge-transfer characteristics, as noted in previous studies [28–30]. Therefore, it can be classified as a bound exciton of the charge-transfer type. In the condensed phase, water molecules construct a tetrahedral structure via H bonding. The H bonding can be described by a Coulombic attraction between the electronegative oxygen on an acceptor molecule and the electropositive proton on a donor molecule, as illustrated in Fig. 3(a). During the process of optical absorption, electron-hole pair excitation also occurs between the donor and acceptor molecules as shown in Fig. 3(a). An electron of $4a_1$ characteristic is excited in the lowest conduction band, which is an antibonding orbital centered on the protons of a water molecule, and, at the same time, a hole of $1b_1$ character is excited in the highest valence band, which consists of lone pair electrons located in close vicinity of the oxygen atom. Not surprisingly, the resulting exciton strongly couples to the H bonding, which applies an electrostatic field pointing from the donor to the acceptor. In the photoabsorption process, the electron in the lone pair orbitals on the H-bond acceptor molecule is excited onto the antibonding orbital on the H-bond donor molecule. Driven by the Coulombic attraction, the process of electron-hole pair excitation takes place along the H-bonding direction, and a charge-transfer exciton is stabilized on the H-bonded water molecules. As a bipolar molecule, a water molecule serves as both an H-bond donor and an H-bond acceptor, and, therefore, both electron and hole states can be simultaneously found on a single water molecule during an excitation. As a result, large excitonic effects can be seen in Fig. 3(b), which are manifested in the pronounced absorption features and large exciton binding energies of approximately 2.2 eV in water and approximately 3.4 eV in hexagonal ice.

In water, the H bond constantly breaks and reforms on a timescale of picoseconds [36–38]. In its liquid structure, the strength of H bonding undergoes a significant fluctuation as well. The strength of H bonding and its variance in water can be seen in Fig. 3(c) from the broad distribution function of the proton transfer coordinate $\nu = d_{\mathrm{OH}} - d_{\mathrm{O\cdots H}}$ [60,61], where d_{OH} denotes the length of the OH covalent bond and $d_{\mathrm{O\cdots H}}$ denotes the distance between the H atom and the O

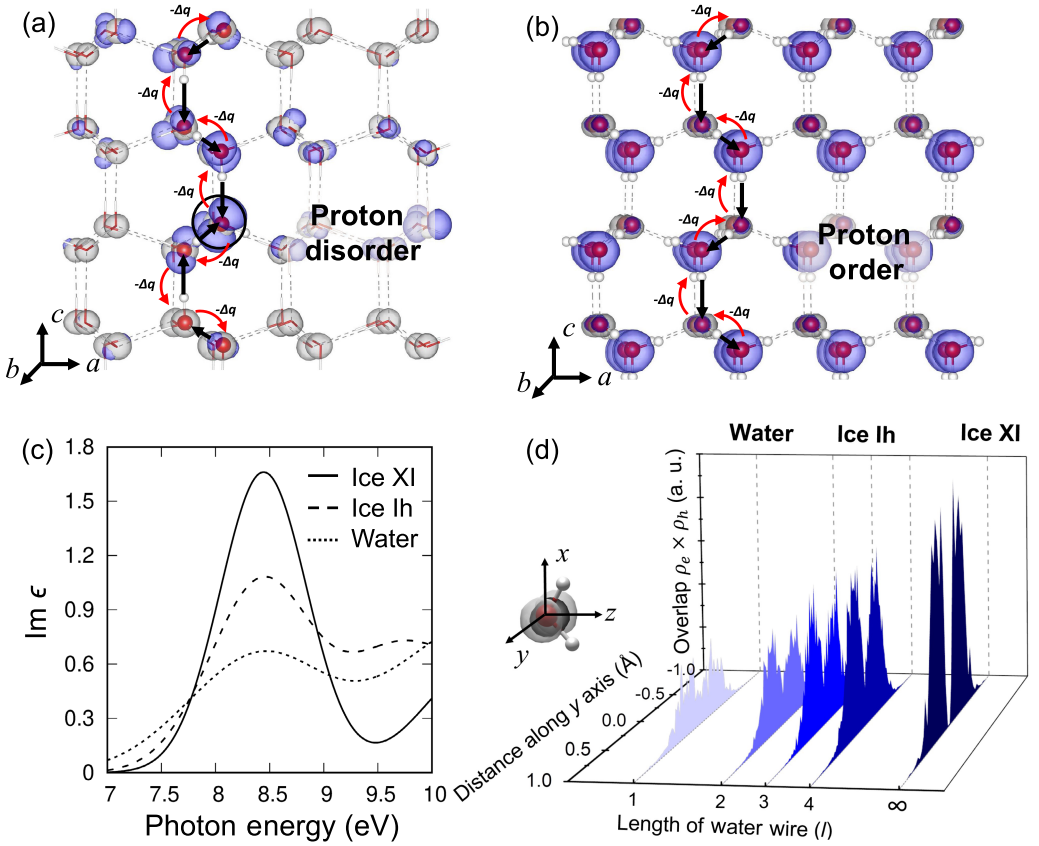

FIG. 4. Exciton corresponding to the first peak of optical spectra and molecular structure of ice I*h* (a) and ice XI (b). The real-space plot is the averaged electron and hole density of the exciton. The blue color denotes the hole density, while the gray color denotes the electron density. The black arrows indicate the direction of the water wire. The red arrows indicate the direction of the charge transfer. The black circle shown in (a) marks the position where the proton disorder happens. (c) The first peak of the theoretical optical spectra of ice XI (solid line), ice I*h* (dashed line), and liquid water (dotted line). (d) Three-dimensional plot of the overlap between hole density and electron density ($\rho_h \times \rho_e$) of the excitons in the first peaks of spectra of water, ice I*h*, and ice XI, with respect to the length of the water wire. The x-z plane is parallel to the water molecule. The zero point of the y axis is set at the position of the oxygen atom.

atom in the H-bond acceptor. By convention, ν has been adopted in Fig. 3(a) as a descriptor to represent the H-bonding strength, where a more positive (negative) ν means a physically stronger (weaker) H-bonding strength between two neighboring water molecules. Because of its coupling to the H bonding, it is expected that the charge-transfer exciton and its spectral signals are sensitive to its H-bonding environment in liquid. In Fig. 3(c), we present the electron-hole overlap function ($\rho_h \times \rho_e$) as a function of H-bonding strength in terms of the proton transfer coordinate ν for each pair of neighboring water molecules averaged by using many configurations which are extracted from molecular dynamics simulation trajectories. The electron-hole overlap function is computed from the sum of the product of electron and hole densities obtained from BSE eigenstates whose excitation energies are located within the first absorption peak at approximately 8 eV, and the electron-hole overlap function has been averaged over the pair of neighboring water molecules. The details of the calculations of the electron and hole densities can be found in Sec. III in Supplemental Materials [51]. In Fig. 3(c), a strong correlation between a charge-transfer exciton and its H-bonding strength can be clearly identified. When the H bonding between two water molecules is relatively weak in Fig. 3(c), the hole and electron barely overlap with each other and, therefore, contribute little to the observed absorption spectra. As the H bonding become stronger, the polarization field greatly facilitates the electron-hole excitation and their overlap on the H-bonded water molecule, yielding a significant increase in optical oscillator strength. Our analysis shows that the first spectral peak is dominated by charge-transfer excitons on pairs of water molecules with nearly ideal H-bonding strength comparable to the H-bonding strengths in hexagonal ice.

C. Collective excitation of charge-transfer excitons on water wires

Under ambient pressure, the crystalline structure of regular ice I*h* can be viewed as an assembly of corrugated oxygen bilayers stacked on top of each other as shown in Fig. 4(a). In ice I*h*, the oxygen atoms are located on lattice sites satisfying hexagonal symmetry, while the protons take

nearly random positions that are allowed by the *ice rule* [52,53], which is referred to as proton disorder in the field [62,63]. In ice, all neighboring water molecules are H bonded, and the bonding strength of $\nu \simeq -0.70$ in ice is much stronger than the average bonding strength of $\nu \simeq -0.85$ in liquid water. These intact H bonds not only construct an extended tetrahedral structure, but also become interconnected among themselves and form persistent water wires on their underlying H-bond network. As shown in Fig. 4(a), we present a typical water wire in regular ice. Along this water wire, five water molecules on the top three bilayers are threaded by four consecutive H bonds in a zigzag chain. Because of the highly directional nature of H bonding, a water wire can be defined to be a proton-ordered chain if all the participating H bonds adopt the same bonding direction pointing from donor molecule to acceptor molecule along the wire, or vice versa. As such, the above prototypical water wire can be assigned with an ordering length ($l = 4$) from the number of constituent H bonds and with an ordering direction which is along the c axis of the hexagonal lattice. The ordering of the above water wire is interrupted by a proton disorder occurring at the bottom bilayer as denoted by the black circle in Fig. 4(a). Therefore, only finite-sized proton-ordered water wires exist, whose lengths and locations are randomly distributed in ice Ih.

In ice Ih, the presence of water wires greatly enhances excitonic effects at the main peak in the optical absorption spectrum. On a proton-ordered water wire, the H bonds are connected head to tail along its ordering direction, and each water molecule in ice carries an electric dipole approximately $3.09D$ along a direction roughly bisecting its covalent bond angle. In compliance with the ordering, the water molecules on a wire also position themselves in a structured configuration. As a result, the axes of the individual electric dipoles of water molecules on the wire are aligned as well, yielding a polar ordering along the c axis as shown in Fig. 4(b). Because of the proton disorder, the polar ordering occurs on water wires of random sizes and random direction in regular ice. Therefore, no ferroelectricity exists [1,7,64], and ice Ih remains paraelectric. Nevertheless, along an ordered water wire, a local polarization field arises. In ice Ih, the charge-transfer exciton is not only promoted by its intact H bonds, but also further stabilized by the local polarization field along the wire. As a result, the main peak of the optical absorption spectrum in ice Ih is mainly characterized by a collective exciton excitation of charge-transfer type on a proton-ordered water wire as shown in Fig. 4(c). In this collective excitation, a relay of electron-hole pairs takes place. For a water molecule along the wire, a hole state is generated at the $1b_1$ valence orbital centered on an oxygen atom by passing electrons onto the $4a_1$ empty orbital at the hydrogen atom of one of the neighboring molecules, and simultaneously the empty state of the same molecule receives electrons from the other neighboring molecule as shown in Fig. 4(b). Here, the proton-ordered water wire plays a key role in stabilizing the collective charge-transfer exciton, since its polarization field tilts the energy landscape in favor of formation of an electron and a hole on the H-bond acceptor and donor molecules, respectively, and creates a potential that reduces recombination. In the liquid water, the H bond constantly breaks and reforms. Therefore, it cannot contain any long water wire ($l > 2$), and the number of water wires stays roughly constant with respect to temperature, since they are dominated by pairs of molecules forming H bonds at all temperatures. Indeed, as shown in Fig. S4 in Supplemental Material [51], the first peak of the optical spectra in liquid water at different temperatures is almost identical. Since, the polarization field increases with the ordering length of a water wire before reaching a limit (see Sec. VIII in Supplemental Material [51]), the collective exciton is expected to be more stabilized on a water wire with longer ordering length. Indeed, the overlap density of electron-hole pairs clearly increases when ordering length (l) increases as plotted in Fig. 4(d), which correlates with an enhanced exciton oscillator strength. Consistently, the collective excitation on water wires in ice Ih results in a stronger binding energy of approximately 3.4 eV compared with that in water of approximately 2.2 eV as well as a more pronounced absorption intensity as shown in Fig. 4(c).

At temperatures below 80 K, ice XI, a proton-ordered hexagonal phase [7,64], becomes energetically more stable relative to ice Ih. In the absence of proton disorder, the water wires in ice XI develop a long-range ordering length ($l = \infty$) along the c axis. On this ordered water wire with ($l = \infty$), the aligned electric dipoles maximize the polarization field and yield a ferroelectricity with $P \simeq 21\ \mu\mathrm{C/cm^2}$ along the c axis of the hexagonal crystal. Not surprisingly, excitonic effects are also maximized, which is evidenced by the large increase in the magnitude of the electron-hole overlap density at $l = \infty$ in Fig. 4(d). As expected, the binding energy of the main peak increases to approximately 3.6 eV relative to approximately 3.4 eV in ice Ih, and its intensity is also the most pronounced among all the solid and liquid phases of water under current investigation as shown in Fig. 4(c).

IV. CONCLUSION

Based on theoretical calculations of the optical absorption spectra of liquid water and ices within *ab initio* many-body perturbation theory, we elucidate the structural signatures of the H-bond network in experimentally observed spectral features. The main peak in the optical spectra is a charge-transfer-type exciton and is strongly coupled to the H-bonding strength. In water, a relatively strong H bonding under thermal fluctuation promotes a strong excitonic effect with a pronounced oscillator strength. In ice, the presence of water wires further

enhances the electron-hole interaction via a collective exciton excitation facilitated by the polarization field from the aligned electric dipoles. The collective exciton excitation is also sensitive to the ordering length of the water wire. As demonstrated in water, regular ice, and ice XI, the increasing oscillator strength of the main exciton peak can be interpreted as a signature of short-range, intermediate-range, and long-range ordered water wires. Based on this approach, the water wires in physiological systems [3,5,8], under nanoconfinement [6,9,65,66], and in the rich phase diagram of solid ices [67–71] can be probed and interpreted by optical absorption spectroscopy, opening pathways for the optical detection and characterization of energy, charge, and information transfer in aqueous environments.

ACKNOWLEDGMENTS

This work was supported by the Computational Chemical Center: Chemistry in Solution and at Interfaces funded by the U.S. Department of Energy under Grant No. DE-SC0019394. D. Y. Q. was supported by the National Science Foundation (NSF) Condensed Matter and Materials Theory (CMMT) program under Career Grant No. DMR-2337987 and Grant No. DMR-2114081. Development of the BerkeleyGW code was supported by Center for Computational Study of Excited-State Phenomena in Energy Materials (C2SEPEM) at the Lawrence Berkeley National Laboratory, funded by the U.S. Department of Energy, Office of Science, Basic Energy Sciences, Materials Sciences and Engineering Division, under Contract No. DE-AC02-05CH11231. The computational work used resources of the National Energy Research Scientific Computing Center (NERSC), a U.S. Department of Energy Office of Science User Facility operated under Contract No. DE-AC02-05CH11231. This research used resources of the Oak Ridge Leadership Computing Facility at the Oak Ridge National Laboratory, which is supported by the Office of Science of the U.S. Department of Energy under Contract No. DE-AC05-00OR22725. This research includes calculations carried out on Temple University's HPC resources and, thus, was supported in part by the National Science Foundation through major research instrumentation Grant No. 1625061 and by the U.S. Army Research Laboratory under Contract No. W911NF-16-2-0189.

[1] X. Su, L. Lianos, Y. R. Shen, and G. A. Somorjai, *Surface-induced ferroelectric ice on pt(111)*, Phys. Rev. Lett. **80**, 1533 (1998).

[2] C. Dellago, M. M. Naor, and G. Hummer, *Proton transport through water-filled carbon nanotubes*, Phys. Rev. Lett. **90**, 105902 (2003).

[3] E. Freier, S. Wolf, and K. Gerwert, *Proton transfer via a transient linear water-molecule chain in a membrane protein*, Proc. Natl. Acad. Sci. U.S.A. **108**, 11435 (2011).

[4] A. Hassanali, M. K. Prakash, H. Eshet, and M. Parrinello, *On the recombination of hydronium and hydroxide ions in water*, Proc. Natl. Acad. Sci. U.S.A. **108**, 20410 (2011).

[5] J. Paulino, M. Yi, I. Hung, Z. Gan, X. Wang, E. Y. Chekmenev, H. X. Zhou, and T. A. Cross, *Functional stability of water wire-carbonyl interactions in an ion channel*, Proc. Natl. Acad. Sci. U.S.A. **117**, 11908 (2020).

[6] C. Li and G. A. Voth, *A quantitative paradigm for water-assisted proton transport through proteins and other confined spaces*, Proc. Natl. Acad. Sci. U.S.A. **118**, 1 (2021).

[7] J. Lasave, S. Koval, A. Laio, and E. Tosatti, *Proton strings and rings in atypical nucleation of ferroelectricity in ice*, Proc. Natl. Acad. Sci. U.S.A. **118**, e2018837118 (2021).

[8] H. T. Kratochvil, L. C. Watkins, M. Mravic, J. L. Thomaston, J. M. Nicoludis, N. H. Somberg, L. Liu, M. Hong, G. A. Voth, and W. F. Degrado, *Transient water wires mediate selective proton transport in designed channel proteins*, Nat. Chem. **15**, 1012 (2023).

[9] G. Hummer, *Water, proton, and ion transport: From nanotubes to proteins*, Mol. Phys. **105**, 201 (2007).

[10] B. Halle and G. Karlström, *Prototropic charge migration in water. Part 2—Interpretation of nuclear magnetic resonance and conductivity data in terms of model mechanisms*, J. Chem. Soc., Faraday Trans. 2 **79**, 1047 (1983).

[11] C. W. Swartz and X. Wu, *Ab initio studies of ionization potentials of hydrated hydroxide and hydronium*, Phys. Rev. Lett. **111**, 087801 (2013).

[12] G. Bekçioğlu, C. Allolio, and D. Sebastiani, *Water wires in aqueous solutions from first-principles calculations*, J. Phys. Chem. B **119**, 4053 (2015).

[13] N. Agmon, H. J. Bakker, R. K. Campen, R. H. Henchman, P. Pohl, S. Roke, M. Thämer, and A. Hassanali, *Protons and hydroxide ions in aqueous systems*, Chem. Rev. **116**, 7642 (2016).

[14] M. Chen, L. Zheng, B. Santra, H. Y. Ko, R. A. Distasio, M. L. Klein, R. Car, and X. Wu, *Hydroxide diffuses slower than hydronium in water because its solvated structure inhibits correlated proton transfer*, Nat. Chem. **10**, 413 (2018).

[15] A. R. Walker, B. Wu, J. Meisner, M. D. Fayer, and T. J. Martínez, *Proton transfer from a photoacid to a water wire: First principles simulations and fast fluorescence spectroscopy*, J. Phys. Chem. B **125**, 12539 (2021).

[16] F. Tang, J. Xu, D. Y. Qiu, and X. Wu, *Nuclear quantum effects on the quasiparticle properties of the chloride anion aqueous solution within the GW approximation*, Phys. Rev. B **104**, 035117 (2021).

[17] A. K. Soper, *The radial distribution functions of water as derived from radiation total scattering experiments: Is there anything we can say for sure?*, Int. Scholarly Res. Not. **2013**, 279463 (2013).

[18] L. B. Skinner, C. Huang, D. Schlesinger, L. G. M. Pettersson, A. Nilsson, and C. J. Benmore, *Benchmark oxygen-oxygen pair-distribution function of ambient water from x-ray diffraction measurements with a wide Q-range*, J. Chem. Phys. **138**, 074506 (2013).

[19] W. Schmidt, *Optical Spectroscopy in Chemistry and Life Sciences: An Introduction* (Wiley, New York, 2005).

[20] W. W. Parson, *Modern Optical Spectroscopy* (Springer, New York, 2007), Vol. 2.

[21] K. F. Mak, L. Ju, F. Wang, and T. F. Heinz, *Optical spectroscopy of graphene: From the far infrared to the ultraviolet*, Solid State Commun. **152**, 1341 (2012).
[22] P. Wernet, D. Nordlund, U. Bergmann, M. Cavalleri, M. Odelius, H. Ogasawara, L. A. Naslund, T. K. Hirsch, L. Ojamae, P. Glatzel, L. G. M. Pettersson, and A. Nilsson, *The structure of the first coordination shell in liquid water*, Science **304**, 995 (2004).
[23] J. S. Tse, D. M. Shaw, D. D. Klug, S. Patchkovskii, G. Vankó, G. Monaco, and M. Krisch, *X-ray raman spectroscopic study of water in the condensed phases*, Phys. Rev. Lett. **100**, 095502 (2008).
[24] T. Fransson, Y. Harada, N. Kosugi, N. A. Besley, B. Winter, J. J. Rehr, L. G. Pettersson, and A. Nilsson, *X-ray and electron spectroscopy of water*, Chem. Rev. **116**, 7551 (2016).
[25] J. W. Smith and R. J. Saykally, *Soft x-ray absorption spectroscopy of liquids and solutions*, Chem. Rev. **117**, 13909 (2017).
[26] F. Tang, Z. Li, C. Zhang, S. G. Louie, R. Car, D. Y. Qiu, and X. Wu, *Many-body effects in the x-ray absorption spectra of liquid water*, Proc. Natl. Acad. Sci. U.S.A. **119**, e2201258119 (2022).
[27] F. Tang, K. Shi, and X. Wu, *Exploring the impact of ions on oxygen K-edge x-ray absorption spectroscopy in* NaCl *solution using the GW-Bethe-Salpeter-equation approach*, J. Chem. Phys. **159**, 174501 (2023).
[28] P. H. Hahn, W. G. Schmidt, K. Seino, M. Preuss, F. Bechstedt, and J. Bernholc, *Optical absorption of water: Coulomb effects versus hydrogen bonding*, Phys. Rev. Lett. **94**, 037404 (2005).
[29] V. Garbuio, M. Cascella, L. Reining, R. Del Sole, and O. Pulci, *Ab initio calculation of optical spectra of liquids: Many-body effects in the electronic excitations of water*, Phys. Rev. Lett. **97**, 137402 (2006).
[30] A. Hermann, W. G. Schmidt, and P. Schwerdtfeger, *Resolving the optical spectrum of water: Coordination and electrostatic effects*, Phys. Rev. Lett. **100**, 207403 (2008).
[31] A. Hermann and P. Schwerdtfeger, *Blue shifting the onset of optical UV absorption for water under pressure*, Phys. Rev. Lett. **106**, 187403 (2011).
[32] J. Vinson, J. J. Kas, F. D. Vila, J. J. Rehr, and E. L. Shirley, *Theoretical optical and x-ray spectra of liquid and solid* H_2O, Phys. Rev. B **85**, 045101 (2012).
[33] V. Garbuio, M. Cascella, I. Kupchak, O. Pulci, and A. P. Seitsonen, *Proton disorder in cubic ice: Effect on the electronic and optical properties*, J. Chem. Phys. **143**, 084507 (2015).
[34] V. Ziaei and T. Bredow, *Red and blue shift of liquid water's excited states: A many body perturbation study*, J. Chem. Phys. **145**, 064508 (2016).
[35] N. L. Nguyen, H. Ma, M. Govoni, F. Gygi, and G. Galli, *Finite-field approach to solving the Bethe-Salpeter equation*, Phys. Rev. Lett. **122**, 237402 (2019).
[36] M. V. Fernández-Serra and E. Artacho, *Electrons and hydrogen-bond connectivity in liquid water*, Phys. Rev. Lett. **96**, 016404 (2006).
[37] R. Kumar, J. R. Schmidt, and J. L. Skinner, *Hydrogen bonding definitions and dynamics in liquid water*, J. Chem. Phys. **126**, 204107 (2007).
[38] F. Perakis, L. De Marco, A. Shalit, F. Tang, Z. R. Kann, T. D. Kühne, R. Torre, M. Bonn, and Y. Nagata, *Vibrational spectroscopy and dynamics of water*, Chem. Rev. **116**, 7590 (2016).
[39] M. S. Hybertsen and S. G. Louie, *Electron correlation in semiconductors and insulators: Band gaps and quasiparticle energies*, Phys. Rev. B **34**, 5390 (1986).
[40] M. Rohlfing and S. G. Louie, *Electron-hole excitations and optical spectra from first principles*, Phys. Rev. B **62**, 4927 (2000).
[41] J. Deslippe, G. Samsonidze, D. A. Strubbe, M. Jain, M. L. Cohen, and S. G. Louie, *BERKELEYGW: A massively parallel computer package for the calculation of the quasiparticle and optical properties of materials and nanostructures*, Comput. Phys. Commun. **183**, 1269 (2012).
[42] C. Zhang, F. Tang, M. Chen, J. Xu, L. Zhang, D. Y. Qiu, J. P. Perdew, M. L. Klein, and X. Wu, *Modeling liquid water by climbing up Jacob's ladder in density functional theory facilitated by using deep neural network potentials*, J. Phys. Chem. B **125**, 11444 (2021).
[43] J. P. Perdew, K. Burke, and M. Ernzerhof, *Generalized gradient approximation made simple*, Phys. Rev. Lett. **77**, 3865 (1996).
[44] J. P. Perdew, M. Ernzerhof, and K. Burke, *Rationale for mixing exact exchange with density functional approximations*, J. Chem. Phys. **105**, 9982 (1996).
[45] C. Adamo and V. Barone, *Toward reliable density functional methods without adjustable parameters: The PBE0 model*, J. Chem. Phys. **110**, 6158 (1999).
[46] C. Faber, P. Boulanger, I. Duchemin, C. Attaccalite, and X. Blase, *Many-body Green's function GW and Bethe-Salpeter study of the optical excitations in a paradigmatic model dipeptide*, J. Chem. Phys. **139**, 194308 (2013).
[47] F. Caruso, V. Atalla, X. Ren, A. Rubio, M. Scheffler, and P. Rinke, *First-principles description of charge transfer in donor-acceptor compounds from self-consistent many-body perturbation theory*, Phys. Rev. B **90**, 085141 (2014).
[48] F. Kaplan, F. Weigend, F. Evers, and M. J. van Setten, *Off-diagonal self-energy terms and partially self-consistency in GW calculations for single molecules: Efficient implementation and quantitative effects on ionization potentials*, J. Chem. Theory Comput. **11**, 5152 (2015).
[49] M. Ceriotti, G. Bussi, and M. Parrinello, *Nuclear quantum effects in solids using a colored-noise thermostat*, Phys. Rev. Lett. **103**, 030603 (2009).
[50] M. Ceriotti and D. E. Manolopoulos, *Efficient first-principles calculation of the quantum kinetic energy and momentum distribution of nuclei*, Phys. Rev. Lett. **109**, 100604 (2012).
[51] See Supplemental Material at http://link.aps.org/supplemental/10.1103/PhysRevX.15.011048 for detailed information on the molecular dynamics simulation, ground state calculations, and GW-BSE calculations, as well as the analysis of the electron and hole distributions for each exciton state in real space, are provided. Additionally, the decomposed spectra based on the restricted subspace method, determination of the exciton binding energy, temperature dependence of the optical spectra of liquid water, absorption coefficient spectra for both liquid water and ice, local polar fields along the water wire in ice I*h*, and

Supplemental Figures can be found in the Supplemental Material.

[52] J. D. Bernal and R. H. Fowler, *A theory of water and ionic solution, with particular reference to hydrogen and hydroxyl ions*, J. Chem. Phys. **1**, 515 (1933).

[53] A. Rahman and F. H. Stillinger, *Proton distribution in ice and the Kirkwood correlation factor*, J. Chem. Phys. **57**, 4009 (1972).

[54] P. Giannozzi *et al.*, *Advanced capabilities for materials modelling with Quantum ESPRESSO* , J. Phys. Condens. Matter **29**, 465901 (2017).

[55] A. J. Cohen, P. Mori-Sánchez, and W. Yang, *Insights into current limitations of density functional theory*, Science **321**, 792 (2008).

[56] A. J. Cohen, P. Mori-Sánchez, and W. Yang, *Challenges for density functional theory*, Chem. Rev. **112**, 289 (2012).

[57] D. R. Hamann, *Optimized norm-conserving Vanderbilt pseudopotentials*, Phys. Rev. B **88**, 085117 (2013).

[58] H. Hayashi and N. Hiraoka, *Accurate measurements of dielectric and optical functions of liquid water and liquid benzene in the VUV region (1–100 eV) using small-angle inelastic x-ray scattering*, J. Phys. Chem. B **119**, 5609 (2015).

[59] K. Kobayashi, *Optical spectra and electronic structure of ice*, J. Phys. Chem. **87**, 4317 (1983).

[60] M. Ceriotti, J. Cuny, M. Parrinello, and D. E. Manolopoulos, *Nuclear quantum effects and hydrogen bond fluctuations in water*, Proc. Natl. Acad. Sci. U.S.A. **110**, 15591 (2013).

[61] Z. Sun, L. Zheng, M. Chen, M. L. Klein, F. Paesani, and X. Wu, *Electron-hole theory of the effect of quantum nuclei on the x-ray absorption spectra of liquid water*, Phys. Rev. Lett. **121**, 137401 (2018).

[62] S. M. Jackson and R. W. Whitworth, *Thermally-stimulated depolarization studies of the ice XI ice-Ih phase transition*, J. Phys. Chem. B **101**, 6177 (1997).

[63] J.-L. Kuo, M. L. Klein, and W. F. Kuhs, *The effect of proton disorder on the structure of ice-Ih: A theoretical study*, J. Chem. Phys. **123**, 134505 (2005).

[64] Y. Tajima, T. Matsuo, and H. Suga, *Phase transition in KOH-doped hexagonal ice*, Nature (London) **299**, 810 (1982).

[65] V. Kapil, C. Schran, A. Zen, J. Chen, C. J. Pickard, and A. Michaelides, *The first-principles phase diagram of monolayer nanoconfined water*, Nature (London) **609**, 512 (2022).

[66] P. Ravindra, X. R. Advincula, C. Schran, A. Michaelides, and V. Kapil, *Quasi-one-dimensional hydrogen bonding in nanoconfined ice*, Nat. Commun. **15**, 7301 (2024).

[67] P. W. Bridgman, *Water, in the liquid and five solid forms, under pressure*, Proc. Am. Acad. Arts Sci. **47**, 441 (1912).

[68] P. W. Bridgman, *The phase diagram of water to* 45, 000 kg/cm2, J. Chem. Phys. **5**, 964 (1937).

[69] V. F. Petrenko and R. W. Whitworth, *Physics of Ice* (Oxford University Press, New York, 2002).

[70] C. G. Salzmann, P. G. Radaelli, E. Mayer, and J. L. Finney, *Ice XV: A new thermodynamically stable phase of ice*, Phys. Rev. Lett. **103**, 105701 (2009).

[71] L. Zhang, H. Wang, R. Car, and W. E, *Phase diagram of a deep potential water model*, Phys. Rev. Lett. **126**, 236001 (2021).